Broken ergodicity, memory effect, and rejuvenation in Taylor-phase and decagonal $Al_3(Mn,Pd,Fe)$ complex intermetallics

J. Dolinšek,[1] J. Slanovec,[2] Z. Jagličić,[2,3] M. Heggen,[4] S. Balanetskyy,[4] M. Feuerbacher,[4] and K. Urban[4]
[1]*J. Stefan Institute, University of Ljubljana, Jamova 39, SI-1000 Ljubljana, Slovenia*
[2]*Institute of Mathematics, Physics and Mechanics, University of Ljubljana, Jadranska 19, SI-1000 Ljubljana, Slovenia*
[3]*Faculty of Civil and Geodetic Engineering, University of Ljubljana, Jamova 2, SI-1000 Ljubljana, Slovenia*
[4]*Institut für Festkörperforschung, Forschungszentrum Jülich, Jülich, D-52425, Germany*
(Received 25 October 2007; published 26 February 2008)

The Taylor-phase complex intermetallic compound T-Al_3Mn, its solid solutions with Pd and Fe, T-$Al_3(Mn,Pd)$ and T-$Al_3(Mn,Fe)$, and the related decagonal d-Al-Mn-Fe quasicrystal belong to the class of magnetically frustrated spin systems that exhibit rich out-of-equilibrium spin dynamics in the nonergodic phase below the spin-freezing temperature T_f. Performing large variety of magnetic experiments as a function of temperature, magnetic field, aging time t_w, and different thermal histories, we investigated broken-ergodicity phenomena of (i) a difference in the field-cooled and zero-field-cooled susceptibilities, (ii) the frequency-dependent freezing temperature, $T_f(\nu)$, (iii) hysteresis and remanence, (iv) ultraslow decay of the thermoremanent magnetization, (v) the memory effect (a state of the spin system reached upon isothermal aging can be retrieved after a negative temperature cycle), and (vi) "rejuvenation" (small positive temperature cycle within the nonergodic phase erases the effect of previous aging). We show that the phenomena involving isothermal aging periods (the memory effect, rejuvenation, and the ultraslow decay of the thermoremanent magnetization) get simple explanation by considering that during aging under steady external conditions, localized spin regions quasiequilibrate into more stable configurations, so that higher thermal energy is needed to destroy these regions by spin flipping, as compared to the thermal energy required to reverse a frustrated spin in a disordered spin-glass configuration that forms in the case of no aging. Common to all the investigated broken-ergodicity phenomena is the slow approach of a magnetically frustrated spin system toward a global equilibrium, which can never be reached on accessible experimental time scales due to macroscopic equilibration times.

DOI: 10.1103/PhysRevB.77.064430 PACS number(s): 75.50.Lk, 75.47.Np, 71.23.Ft

I. INTRODUCTION

The out-of-equilibrium dynamics of magnetically frustrated systems is one of the challenging fields in condensed matter physics, both theoretically[1,2] and experimentally.[3–5] The dynamics of these systems is characterized by a continuous slowing down of spin fluctuations (reorientations) upon cooling, and frustration implies that there exists a broad spectrum of reorientation times, ranging from microscopic up to the age of the universe. At the spin-freezing temperature T_f, the system undergoes an ergodic-nonergodic phase transition, where below T_f, thermal spin reorientations can no longer maintain thermal equilibrium on the experimentally accessible time scales. Ergodicity of the spin system is consequently broken and the out-of-equilibrium dynamics is associated with the slow approach toward a thermodynamic equilibrium, which can never be reached due to macroscopic equilibration times. Typical broken-ergodicity phenomena observed in magnetically frustrated systems are the following: (i) a large difference between field-cooled (fc) and zero-field-cooled (zfc) magnetic susceptibilities below T_f in small magnetic fields; (ii) the zfc susceptibility exhibits a frequency-dependent cusp associated with a frequency-dependent freezing temperature, $T_f(\nu)$; (iii) there exists an ergodicity-breaking line in the magnetic field–temperature (H-T) phase diagram (the de Almeida–Thouless line); (iv) the third-order nonlinear susceptibility χ_3 shows a sharp anomaly in the vicinity of T_f. The ultraslow approach toward thermal equilibrium in experiments involving isothermal aging periods, where the spin system is let to partially equilibrate during a finite "waiting" (or "aging") time t_w under steady external conditions (temperature and magnetic field), yields additional ergodicity-broken phenomena: (v) a logarithmically slow time decay of the thermoremanent magnetization (TRM), (vi) the memory effect (ME), where a state of the spin system reached upon isothermal aging can be retrieved after a negative temperature cycle, and (vii) "rejuvenation," where small positive temperature cycle within the nonergodic phase erases the effect of previous aging, so that the spin system becomes "young" (unaged) again. The ME is experimentally manifested as a "thermal imprint" in the zero-field-cooled electronic magnetization M_{zfc} at the temperature of aging, which shows depletion (a dip) as compared to M_{zfc} of the no-aging case. The ME and rejuvenation are the most spectacular manifestations of the out-of-equilibrium dynamics of a nonergodic frustrated spin system but are currently incompletely understood (a comprehensive review on the subject can be found in Ref. 5).

The most studied example of magnetically frustrated systems is spin glasses[6] (SGs), denoting site-disordered spin systems that possess (a) frustration (the interaction between spins is such that no configuration can simultaneously satisfy all the bonds and minimize the energy at the same time) and (b) randomness (the spins are positioned randomly in the material). These two properties lead to highly degenerate free-energy landscapes with a distribution of barriers be-

tween different metastable states, resulting in broken ergodicity below T_f. Prototype SGs are canonical spin glasses [dilute magnetic alloys of noble metal host (Cu, Ag, Au) and a magnetic impurity (Fe, Mn)]. Very similar broken-ergodicity phenomena were observed also in pure (site-ordered) geometrically frustrated antiferromagnets (AFMs) with *kagomé* and pyrochlore lattices,[7–11] where triangular or tetrahedral distribution of nearest-neighbor AFM-coupled spins frustrates an ordered periodic system. Rare-earth-containing icosahedral quasicrystals (QCs) Tb-Mg-Zn and Tb-Mg-Cd are other members of the class of geometrically frustrated spin systems,[12,13] where the distribution of localized spins on a quasiperiodic long-range-ordered lattice results in frustration and broken ergodicity.

In this paper, we show that pronounced broken-ergodicity phenomena are present also in the ordered complex intermetallic compound T-Al_3Mn, known as the Taylor (T) phase,[14] its solid solutions with Pd and Fe, T-$Al_3(Mn,Pd)$ and T-$Al_3(Mn,Fe)$, and in their QC-counterpart decagonal phase d-Al-Mn-Fe as well. Performing large variety of magnetic experiments as a function of temperature, magnetic field, aging time t_w, and different thermal histories, we are able to explain the broken-ergodicity phenomena including the ME and rejuvenation on a microscopic level in terms of the out-of-equilibrium dynamics of a nonergodic spin system that tries to come into thermal equilibrium but is ineffective to reach it on the experimentally accessible time scales.

II. SAMPLE SELECTION

Polygrain ingot samples were produced from constituent elements by levitation induction melting in a water-cooled copper crucible under an argon atmosphere. Parts of the samples were annealed in argon at 900 and 930 °C for up to 698 h and subsequently quenched into water. Metallurgical investigations were performed by scanning electron microscopy. Phase compositions were determined by energy-dispersive x-ray analysis (EDX) and, for selected samples, additionally by inductively coupled plasma optical emission spectroscopy. The latter analyses were used for the determination of the oxygen and carbon contents in the samples and for the calibration of the EDX measurements. In addition, the samples were studied by selected-area electron diffraction in a JEOL 4000FX transmission electron microscope operated at 400 kV. Powder x-ray diffraction was carried out on a STOE diffractometer used in transmission mode. Mo $K\alpha_1$ radiation and a position-sensitive detector were used. All annealed samples were single phase. Further details on the preparation, characterization, and structural quality of the samples can be found in a recent publication.[15]

Our study included seven samples, where for all samples the Al concentration was kept constant at 73 at. %. The first sample was a binary T-Al_3Mn of composition $Al_{73}Mn_{27}$ (abbreviated as T-AM in the following). In the T-$Al_3(Mn,Pd)$ series of three samples, a fraction of the magnetic Mn atoms were substituted by nonmagnetic Pd. The compositions (rounded to the closest integer values) of the investigated samples were $Al_{73}Mn_{25}Pd_2$ (T-AMP2), $Al_{73}Mn_{23}Pd_4$ (T-AMP4), and $Al_{73}Mn_{21}Pd_6$ (T-AMP6). In the $Al_3(Mn,Fe)$ series, magnetic Mn atoms were partially substituted by Fe, another magnetic atom. Two samples of compositions $Al_{73}Mn_{25}Fe_2$ (T-AMF2) and $Al_{73}Mn_{23}Fe_4$ (T-AMF4) were T phase, whereas the third sample was a decagonal (d) QC with composition $Al_{73}Mn_{21}Fe_6$ (d-AMF6). All T-phase samples are structurally isomorphic and are considered to be approximants of the decagonal phase. The structure of the binary T-Al_3Mn was first solved by Hiraga *et al.*,[16] whereas the model of T-$Al_3(Mn,Pd)$ with composition $Al_{72.3}Mn_{24.5}Pd_{3.2}$ was reported by Klein *et al.*[17] Within the Klein model,[17] the T-$Al_3(Mn,Pd)$ phase is described as an independent ternary phase structurally similar to binary T-Al_3Mn, whereas Balanetskyy *et al.*[15] have reported that this phase is not an independent ternary phase but a ternary solid solution of Pd in the binary T-Al_3Mn. The structure of the Taylor phase is built of two atomic layers stacked along the b crystallographic axis, a flat layer F, and a puckered layer composed of two sublayers P1 and P2. The orthorhombic unit cell (space group *Pnma*) contains 156 atoms and many of the sites show either fractional occupation (the sites are too close in space to be occupied simultaneously) or mixed Mn/Al occupancy, so that there exists chemical disorder on the lattice. Majority of the atoms are clustered in the form of pentagonal prisms and antiprisms.

III. MAGNETIC SUSCEPTIBILITY AND HYSTERESIS

Magnetic measurements were conducted by a Quantum Design superconducting quantum interference device magnetometer equipped with a 50 kOe magnet, operating in the temperature range 2–300 K. We demonstrate first the broken-ergodicity phenomena by the basic magnetic measurements and then concentrate on the thermoremanent magnetization and the ME and rejuvenation.

A. Zero-field-cooled and field-cooled susceptibilities

In the first set of measurements, zfc and fc susceptibilities $\chi=M/H$ were determined in the temperature range 2–50 K in magnetic fields $H=8$, 50, 100, 1k, 10 k, and 50 kOe. The freezing temperature T_f was determined from the $H=8$ Oe measurements (Fig. 1) as the temperature where the zfc-fc splitting occurred (this coincides well with the temperature where χ_{zfc} exhibits a cusp). The results are collected in Table I, where it is seen that in the T-$Al_3(Mn,Pd)$ series, T_f decreases monotonously with decreasing Mn concentration (from $T_f=24.7$ K in T-AMP2 to $T_f=16.2$ K in T-AMP6), whereas it stays constant at $T_f=22.8\pm0.5$ K for the $Al_3(Mn,Fe)$ series. At T_f, all χ_{zfc}'s exhibit a pronounced cusp, whereas χ_{fc}'s are slightly peaked, indicating critical slowing down of the spin fluctuations in the vicinity of T_f. For the d-AMF6 sample, another anomaly is observed at $T\approx9$ K in both χ_{zfc} and χ_{fc}. The nature of this anomaly is not clear, but the real part of the ac susceptibility (to be presented later) shows that it is frequency dependent, so that it can be associated with another freezing temperature T_{f2}. According to this picture, most spins or clusters in d-AMF6 become nonergodic at the first freezing temperature T_f,

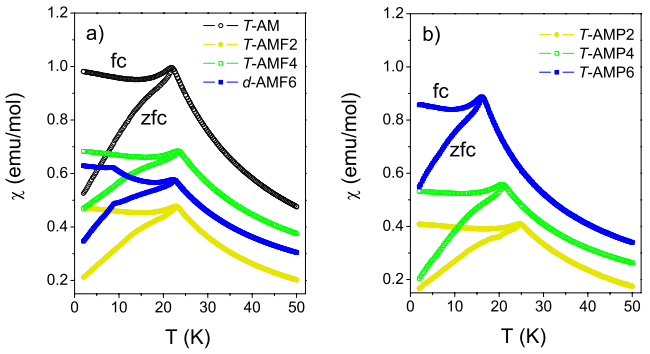

FIG. 1. (Color online) fc and zfc magnetic susceptibilities $\chi = M/H$ of (a) T-AM and T-AMF samples and (b) T-AMP samples in the temperature range 2–50 K and magnetic field $H=8$ Oe. To avoid overlap of the curves, the T-AMF2 curve in panel (a) and the T-AMP2 curve in panel (b) (the two online yellow-colored curves) were shifted down by −0.1 emu/mol on the vertical axis.

whereas some undergo the ergodic-nonergodic transition at a lower temperature T_{f2}.

The H dependence of the zfc-fc susceptibilities [the data for the binary T-AM, representative of all samples, are presented in Fig. 2(a)] reveals the relative strengths of the spin-spin exchange interactions (responsible for magnetic ordering in the absence of an external magnetic field) and the Zeeman interaction of spins with the magnetic field. We observe that for increasing H, the cusp in χ_{zfc} is rounded and the zfc-fc splitting is shifted to lower temperatures until at $H=50$ kOe it almost vanishes [but remains nonzero even at this field, as evident from the inset in Fig. 2(a)]. This shows that the internal magnetic structure is "soft" and fragile with respect to the external magnetic field already at the strength of the order of 10 Oe.

Here, we also mention that in another work[18] on a T-phase sample of composition similar to ours, T-$Al_{73.1}Mn_{21.7}Pd_{5.2}$, a similar, though somewhat lower freezing temperature $T_f=14$ K was reported, whereas diamagnetism was reported for the Mn-poor T-phase sample T-$Al_{78.5}Mn_{16.6}Pd_{4.9}$.

B. Hysteresis

The $M(H)$ curves of the T-AM sample (representative of all seven samples) for the field sweep of ±50 kOe at several temperatures below and above $T_f=22$ K are shown in Figs. 2(b) and 2(c). Hysteresis is observed below T_f at the investigated temperatures 2, 5, and 15 K, and the remanence increases at lower temperatures. This is compatible with the magnetic cluster and/or domain structure of the nonergodic phase. No hysteresis is observed above T_f, not even at 25 K that is only slightly above T_f.

C. Paramagnetic susceptibility

The analysis of the susceptibility $\chi(T)$ in the paramagnetic (ergodic) regime above T_f was performed assuming validity of the Curie–Weiss law, $\chi=C/(T-\theta)$, which gives information on the type and magnitude of magnetic moments through the Curie–Weiss constant C and the type of coupling between the spins through the magnitude and sign of the Curie–Weiss temperature θ. $\chi(T)$ measurements were conducted between 2 and 300 K in $H=1$ kOe and the paramagnetic parameters were extracted from the high-temperature data above 50 K. In Fig. 3, χ^{-1} vs temperature for three representative samples (T-AM, T-AMP2, and d-AMF6) are displayed. The results are collected in Table I, where it is observed that C of the T-$Al_3(Mn,Pd)$ series is decreasing with decreasing Mn concentration, whereas it stays constant for the $Al_3(Mn,Fe)$ series. The Curie–Weiss temperatures of all samples are negative, in the range $-37\ \text{K} < \theta < -10$ K (the values depend somewhat on the analyzed data temperature range), suggesting an AFM-type coupling between the spins.

The decrease of T_f and C upon replacing magnetic Mn by nonmagnetic Pd in the T-$Al_3(Mn,Pd)$ series is consistent with the fact that this substitution results in a dilution of magnetic moments. Similarly, the constancy of these two parameters in the $Al_3(Mn,Fe)$ series can be attributed to a constant number of moments upon replacing magnetic Mn by Fe, another magnetic atom. Mn and Fe in their most common ionization states (Fe^{2+}, Fe^{3+}, Mn^{2+}, Mn^{3+}, and Mn^{4+}) all carry relatively similar magnetic moments between 4.0 and 5.9 μ_B, so that the Mn→Fe substitution does not change significantly the electronic magnetization of the system. The monotonous decrease of T_f and C with decreasing Mn concentration in the Mn→Pd substitution and the constancy of these two parameters in the Mn→Fe substitution suggest

TABLE I. Freezing temperature T_f, Curie constant C, Curie–Weiss temperature θ, average magnetic moment per magnetic atom $\bar{\mu}_{eff}$, and relative change of T_f per decade ν for the investigated Taylor-phase and decagonal QC samples.

Sample	Abbreviation	T_f (K)	C (emu K/mol)	θ (K)	$\bar{\mu}_{eff}$ (μ_B)	$\frac{\Delta T_f}{T_f \Delta(\log \nu)}$
T-$Al_{73}Mn_{27}$	T-AM	22.0	25.9	−11	2.8	0.010
T-$Al_{73}Mn_{25}Pd_2$	T-AMP2	24.7	22.0	−32	2.7	0.010
T-$Al_{73}Mn_{23}Pd_4$	T-AMP4	21.1	20.2	−10	2.7	0.011
T-$Al_{73}Mn_{21}Pd_6$	T-AMP6	16.2	18.1	−23	2.6	0.011
T-$Al_{73}Mn_{25}Fe_2$	T-AMF2	22.9	22.2	−33	2.6	0.010
T-$Al_{73}Mn_{23}Fe_4$	T-AMF4	23.3	22.6	−37	2.7	0.010
d-$Al_{73}Mn_{21}Fe_6$	d-AMF6	22.3	22.6	−23	2.6	0.010

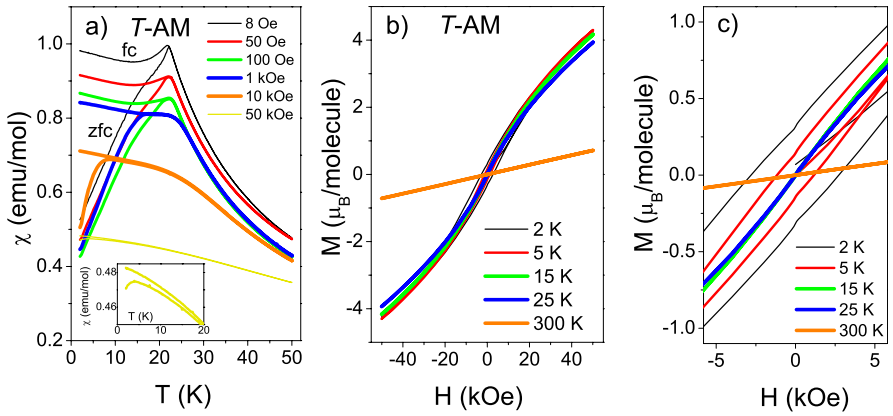

FIG. 2. (Color online) (a) Magnetic field dependence of the zfc and fc susceptibilities in the range $0<H<50$ kOe for the T-AM sample. To avoid overlap of the curves, the 50 Oe curve (online red-colored) was shifted upward by 0.05 emu/mol. The inset shows the zfc-fc splitting of the 50 kOe curve on an expanded scale. (b) $M(H)$ hysteresis curves for this sample at different temperatures below and above $T_f=22.0$ K (a "molecule" denotes one $Al_{73}Mn_{27}$ unit). (c) Expanded portions of the $M(H)$ curves from panel (b) in the vicinity of $H=0$. The hysteresis of the 15 K curve (online green colored) is different from zero but so small that it is not noticeable on the graph.

that majority (perhaps all) of the Mn and Fe atoms carry magnetic moments.

Curie constants from Table I were used to calculate the mean effective magnetic moment $\bar{\mu}_{eff}=\bar{p}_{eff}\mu_B$ per magnetic ion (Mn or Mn+Fe) in the samples. Here, $\bar{p}_{eff}$ is the mean effective Bohr magneton number that can be calculated from the Curie constant using the formula[19] $\bar{p}_{eff}=2.83\sqrt{C}$. All samples show very similar average magnetic moments per magnetic ion $\bar{\mu}_{eff}=(2.7\pm0.1)\mu_B$ (Table I) that are significantly reduced (by a factor about 2) with respect to the values expected for the bare Mn and Fe ions. This indicates that magnetic moments are partially screened by the conduction-electron cloud in a conducting environment.

D. ac susceptibility

The ac susceptibility was measured in an ac magnetic field of amplitude $H_0=6.5$ Oe at frequencies $\nu=1$, 10, 100, and 1000 Hz. The real part of the susceptibility χ' is displayed in Figs. 4(a)–4(c) for three representative samples

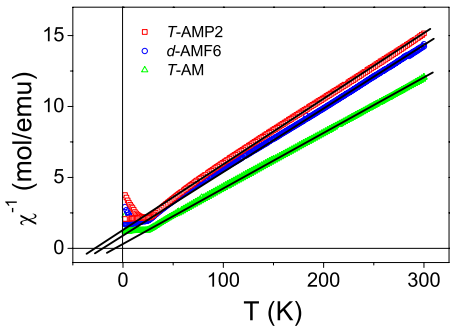

FIG. 3. (Color online) Magnetic susceptibility $\chi(T)$ measurements between 2 and 300 K in $H=1$ kOe for three representative samples (T-AM, T-AMP2, and d-AMF6) in the χ^{-1} vs T plot. Solid lines are Curie–Weiss fits $\chi^{-1}=(T-\theta)/C$ above 50 K (the temperature-independent term χ_0 due to Larmor and Landau diamagnetisms and Pauli paramagnetism is much smaller than the Curie–Weiss term and was neglected in the analysis).

T-AM, T-AMP4, and d-AMF6. As expected for nonergodic spin systems, the position of the cusp in χ' is frequency dependent, shifting to lower temperatures at lower frequencies. For the d-AMF6 sample, the additional anomaly at 9 K is clearly evident, also showing a frequency-dependent shift toward lower temperature for lower frequencies [inset in Fig. 4(c)]. As already discussed, this anomaly is very likely a second freezing temperature T_{f2}.

Considering the cusp in χ' to occur at the freezing temperature, $T_f(\nu)$ relation was determined for all samples by finding the maximum in the second-order polynomial fit through the highest five data points of the $\chi'(\nu)$ curves. $T_f(\nu)$ normalized to the $T_f(1\ \text{Hz})$ value for the T-AMP4 sample is displayed as an inset in Fig. 4(b), where a logarithmic dependence (base 10) of T_f on frequency is evident. The frequency shift of T_f is often quantitatively evaluated by the empirical criterion $\Delta T_f/T_f\Delta(\log\nu)$, i.e., by calculating the relative change of T_f per decade ν. The results are given in Table I, showing that all seven samples show practically the same value, 0.01, which is in the range found for metallic SGs[20] such as AuFe and PdMn. The change of T_f in the investigated frequency range is thus very small, amounting 1% per decade ν. The frequency shift of T_{f2} in the d-AMF6 sample [inset in Fig. 4(c)] is almost the same, $\Delta T_{f2}/T_{f2}\Delta(\log\nu)=0.014$.

IV. THERMOREMANENT MAGNETIZATION

A spectacular manifestation of nonergodicity in magnetically frustrated systems is the observation of aging effects in the ultraslow TRM time decay.[21,22] In this experiment [Fig. 5(a)], one cools the sample in a field H_{fc} from above T_f to a measuring (and, at the same time, aging) temperature $T_1<T_f$, where the spin system is let to age for a time t_w. After t_w, the field H_{fc} is cut to zero and the magnetization time decay is measured over macroscopic times. Upon $H_{fc}\rightarrow0$, the reversible part of the field-cooled magnetization M_{fc} decays to zero almost instantaneously, whereas the irreversible part (the TRM) decays very slowly, typically much slower

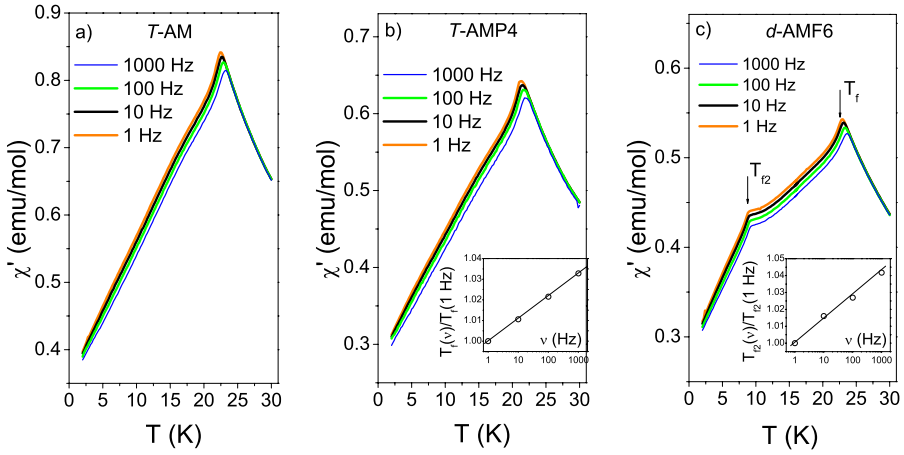

FIG. 4. (Color online) Real part χ' of the ac susceptibility measured in an ac magnetic field $H_0=6.5$ Oe at frequencies $\nu=1$, 10, 100, and 1000 Hz for three representative samples (a) T-AM, (b) T-AMP4, and (c) d-AMF6. The inset in (b) shows $T_f(\nu)$ normalized to $T_f(\nu=1$ Hz). In (c), additional anomaly at 9 K is evident, which is very likely a second freezing temperature T_{f2}. The frequency dependence of this anomaly, $T_{f2}(\nu)/T_{f2}(1\ \mathrm{Hz})$, is shown in the inset in (c). T_{f2} was determined from the minimum in the second derivative $d^2\chi'/dT^2$.

than any experimentally accessible observation time. TRM is a fraction of M_{fc} prior to cutting the field H_{fc} to zero and, depending on temperature, its magnitude amounts from a few percent up to the almost full M_{fc}. The TRM decay depends on the aging temperature T_1, the aging time t_w, and the field H_{fc} in which the aging is performed. Below, we elaborate these dependencies for our investigated samples in detail.

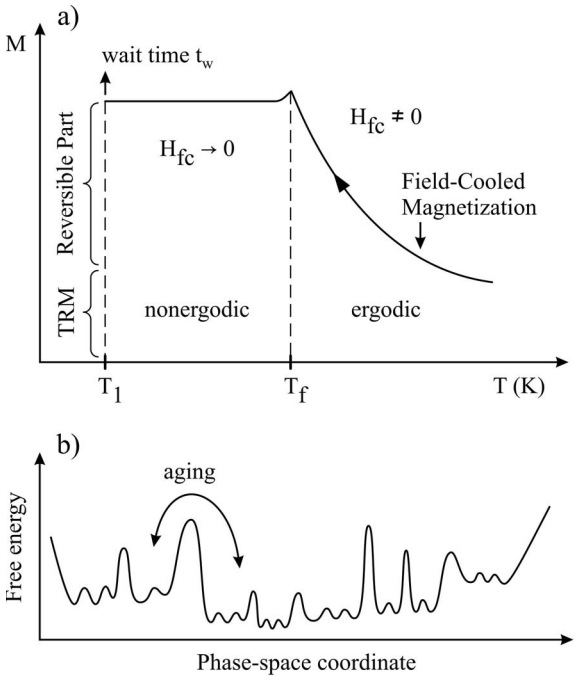

FIG. 5. (a) Protocol for the TRM time-decay measurement. The sample is cooled in a field H_{fc} from above T_f to the aging temperature $T_1<T_f$. At T_1, one waits a time t_w before reducing the field H_{fc} to zero. Following $H_{fc}\to 0$, there is a rapid decay of the reversible part of the magnetization, followed by a slow decay of the irreversible part (the TRM). (b) Coarse-grained free-energy surface of a magnetically frustrated spin system, exhibiting many degenerate local and global minima, separated by a distribution of energy barriers. Aging denotes jumping of the system over the potential barriers during the aging interval t_w.

A. Thermoremanent magnetization versus aging temperature T_1

In the first set of experiments (TRM versus T_1), the samples were cooled in the field $H_{fc}=100$ Oe from the starting temperature 100 K to different measuring temperatures $T_1=5$, 15, and 25 K, where the last temperature was already above T_f. At T_1, aging for $t_w=5000$ s was employed and the TRM decay was monitored for a time $t\approx 240$ min after the H_{fc} switch off. The decay curves normalized to the magnetization prior to cutting the field to zero, $M_{TRM}(T_1,t)/M_{fc}(T_1)$, are displayed in Fig. 6 for two representative samples T-AMP2 ($T_f=24.7$ K) and T-AMF4 ($T_f=23.3$ K). The following observations are evident: (1) the magnitude of the TRM is larger at lower temperature, as a consequence of the increased remanence upon cooling in the nonergodic phase; (2) no TRM was detected at 25 K, which is only slightly above T_f, demonstrating that there is no "smearing" of the ergodic-nonergodic transition into the paramagnetic phase; (3) the TRM decays are logarithmically slow in time t.

B. Thermoremanent magnetization versus aging time t_w

In the second set of experiments, TRM decays were measured as a function of the aging time t_w. The samples were field cooled as before to $T_1=19$ K in $H_{fc}=8$ Oe and were left to age in this field for $t_w=0$, 10, 20, 30, 40, 50, 60, 90, 120, 240, and 600 min. After $H_{fc}\to 0$, the TRM time decays were monitored up to $t=200$ min. The normalized decay curves $M_{TRM}(t_w,t)/M_{fc}(t_w)$ for the samples T-AM ($T_f=22.0$ K) and d-AMF6 ($T_f=22.3$ K) are displayed in Figs. 7(a) and 7(b), showing that the TRM magnitude increases for increasing t_w. In addition, the shape of the TRM decays is also changing with t_w, where for longer t_w, the decays slow down and the

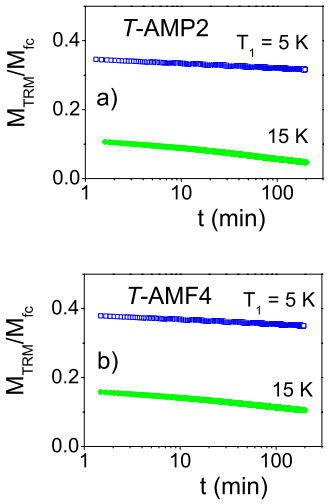

FIG. 6. (Color online) Normalized TRM time decays, M_{TRM}/M_{fc}, as a function of the aging temperature T_1 for two representative samples (a) T-AMP2 (T_f=24.7 K) and (b) T-AMF4 (T_f=23.3 K). Cooling and aging were performed in H_{fc}=100 Oe and the aging time t_w=5000 s was employed. Measurements were performed at T_1=5, 15, and 25 K. Since no TRM was detected at 25 K, the data are not shown.

remanence increases. This is evident from the inset in Fig. 7(a), where the values of the TRM for the T-AM sample taken at different decay times (t=3, 10, and 120 min) are plotted as a function of t_w. The curve at t=120 min clearly grows slower as a function of t_w than the curves at t=3 and 10 min.

C. Thermoremanent magnetization versus cooling field H_{fc}

In the third set of experiments, TRM time decays were measured as a function of the cooling field H_{fc} in which the aging took place. The samples were field cooled to T_1 =19 K and left there to age for t_w=30 min before cutting the field to zero. The following field values were employed: H_{fc}=−8, −4, 2, 4, 8, 50, 100, and 200 Oe. The TRM decays normalized to M_{fc} are displayed in Figs. 8(a) and 8(b) for the T-AM and d-AMF6 samples. We observe that the normalized TRM decreases quite strongly with increasing H_{fc}. The TRM amplitude $M_{TRM}(H_{fc},t)/M_{fc}(H_{fc})$ as a function of H_{fc} for the d-AMF6 sample, taken at the decay time t=120 min, is displayed as an inset in Fig. 8(b), where a decrease by a factor of 2 in the range $0<H_{fc}<200$ Oe is evident. Such a decreasing behavior was also found in a canonical SG CuMn (with 5 at. % Mn),[22] whereas the normalized TRM was found to be H_{fc} independent in the geometrically frustrated icosahedral Tb-Mg-Zn and Tb-Mg-Cd QCs,[13] which was attributed to a superparamagnetic-cluster structure of the magnetic phase in these QC compounds.

The above-presented behavior of the TRM on the aging temperature T_1, the aging time t_w, and the aging field H_{fc} originate from the out-of-equilibrium dynamics of the spin system that approaches thermal equilibrium within two subsequent time intervals in one TRM-decay experiment. During the aging interval (waiting for a t_w in a field H_{fc}), the system approaches an equilibrium state with nonzero magnetization M_{fc} in a field H_{fc}. After the field is cut to zero, the new thermodynamic equilibrium becomes a state with zero magnetization in H_{fc}=0 and the spin system proceeds toward this state during the decay time interval t. Further discussion is deferred and will be performed together with the discussion of the ME and rejuvenation, to be presented next, using a unified physical picture.

V. MEMORY EFFECT AND REJUVENATION

The most spectacular manifestation of the out-of-equilibrium dynamics of a nonergodic magnetically frustrated spin system is the memory effect, where a state of the spin system reached at a given temperature upon isothermal aging for a time t_w can be retrieved after a negative tempera-

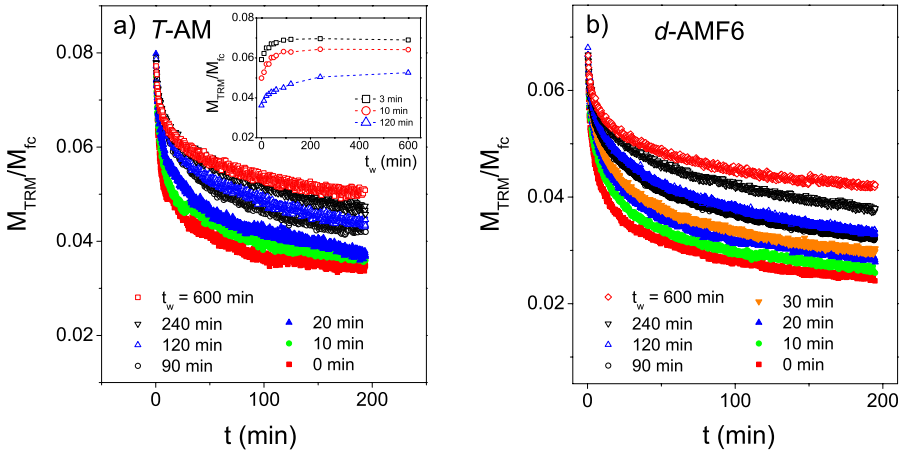

FIG. 7. (Color online) Normalized TRM time decays, M_{TRM}/M_{fc}, as a function of the aging time t_w for two representative samples (a) T-AM (T_f=22.0 K) and (b) d-AMF6 (T_f=22.3 K). The samples were field cooled to T_1=19 K in H_{fc}=8 Oe, where aging was performed for t_w=0, 10, 20, 30, 40, 50, 60, 90, 120, 240, and 600 min. For clarity, not all t_w curves are shown on the graphs. For longer t_w's, the decays slow down and the remanence increases, which is evident from the inset in (a), where the values of the TRM at different decay times (t =3, 10, and 120 min) are plotted as a function of t_w.

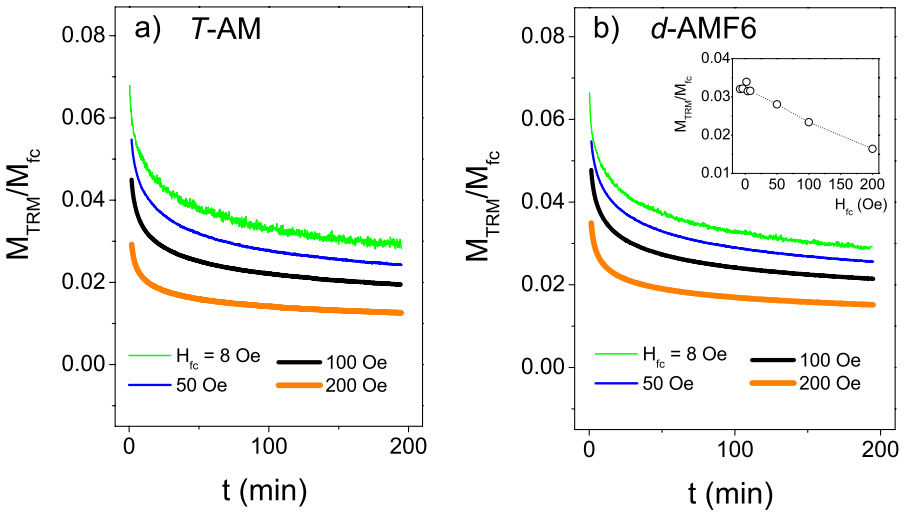

FIG. 8. (Color online) Normalized TRM time decays, M_{TRM}/M_{fc}, as a function of the cooling field H_{fc} for two representative samples (a) T-AM (T_f=22.0 K) and (b) d-AMF6 (T_f=22.3 K). The samples were field cooled to T_1=19 K and left to age in the fields H_{fc}=−8, −4, 2, 4, 8, 50, 100, and 200 Oe for t_w=30 min before cutting the field to zero. For clarity, not all H_{fc} curves are shown on the graphs. A decreasing behavior of the normalized TRM (taken at a decay time t=120 min) with increasing H_{fc} is demonstrated in the inset in (b).

ture cycle. In contrast, small positive temperature cycle erases previous aging, the phenomenon known as rejuvenation. In the ME experiment, the spin system is cooled continuously from the paraphase below the freezing temperature T_f in zero magnetic field and the cooling is stopped at $T_1 < T_f$ for a time t_w of the order of minutes to hours. The cooling then resumes to the lowest temperature where a small magnetic field is applied and the zfc magnetization is measured in a continuous heating run. The memory is imprinted in M_{zfc}, which shows a dip at the temperature T_1 of aging. Heating the system to a higher temperature $T_2 > T_1$, while remaining in the nonergodic phase ($T_2 < T_f$), rejuvenates the system, i.e., the zfc magnetization measured in a subsequent zfc experiment starting from T_2 with no aging at T_1 is again that of the young (unaged) system. The microscopic nature of this "thermally induced magnetic inscription" that is created in the absence of any external magnetic field (note that a low magnetic field is only used for the memory readout upon measuring M_{zfc} in a heating run) is currently incompletely understood.

The ME has been so far most studied in magnetically frustrated systems such as the conducting CuMn canonical SG,[4] insulating Heisenberg-like SG[23] $CdCr_{1.7}In_{0.3}S_4$, Ising-like SG[24] $Fe_{0.5}Mn_{0.5}TiO_3$, interacting Fe-C nanoparticle system,[25] and zinc ferrite nanoparticles.[26] ME is, however, not restricted to magnetically frustrated systems. It was also observed in the dielectric permittivity of electrically frustrated orientational glasses methanol (73%)-β-hydroquinone clathrate[27] and $K_{0.989}Li_{0.011}TaO_3$,[28,29] as well as in disordered ferroelectrics $KTa_{0.973}Nb_{0.027}O_3$ (Ref. 30) and $Pb(Mg_{1/3}Nb_{2/3})O_3$,[31] but in dielectrics the effect is less pronounced than in magnetically frustrated systems. Here, we present the ME in the investigated T-phase family of intermetallics and the decagonal QC. We elaborate the ME in detail by performing a variety of experiments on three representative samples, the binary T-AM and the ternary T-AMP4 and d-AMF6.

A. Memory effect for a one-temperature stop

In the first set of experiments, the samples were zero field cooled continuously from the starting temperature 100 K through T_f into the nonergodic phase with a cooling rate of 2 K/min. At the "stop" temperature T_1=12 K, the cooling was temporarily stopped and the spin system was let to age isothermally for times t_w=10 min, 1 h, and 4 h, and then the cooling resumed to 2 K. A reference run with no stop (t_w=0) at T_1 was also performed. At the lowest temperature, a small magnetic field H_{zfc}=2 Oe was applied (this field value was then used in all further ME experiments) and M_{zfc} was measured in a subsequent heating run to a temperature above T_f.

Figure 9(a) shows the M_{zfc}'s for the T-AM sample, where the ME in the vicinity of T_1=12 K is manifested as a drop of M_{zfc} of the aged curves with respect to the reference (unaged) curve $M_{zfc}(t_w=0)$. Figure 9(b) shows an expanded portion of the curves in the vicinity of T_1, where it is observed that the ME is stronger (the drop of M_{zfc} is larger) for longer aging times. In Fig. 9(c), the normalized difference between the reference curve and the curves with aging at T_1, $\Delta M = [M_{zfc}(t_w=0) - M_{zfc}(t_w)]/M_{zfc}(t_w=0)$, is displayed, where it is seen that the difference for the longest t_w=4 h amounts ΔM=5%. It is interesting to notice that ΔM resembles a resonant curve, being peaked at the aging temperature T_1 =12 K and smeared over a finite temperature interval between 9 and 14 K. Therefore, the investigated T-AM spin system remembers the temperature where the cooling was temporary stopped and also "knows" for how long it has been stopped. It is remarkable that the majority of the memory imprint at T_1 happens already within the short initial aging interval of t_w=10 min, whereas longer aging adds relatively little to the ME (note the small difference between the t_w=1 and 4 h curves in Fig. 9).

The same ME experiments were repeated on the T-AMP4 (Fig. 10) and d-AMF6 (Fig. 11) samples. The results are

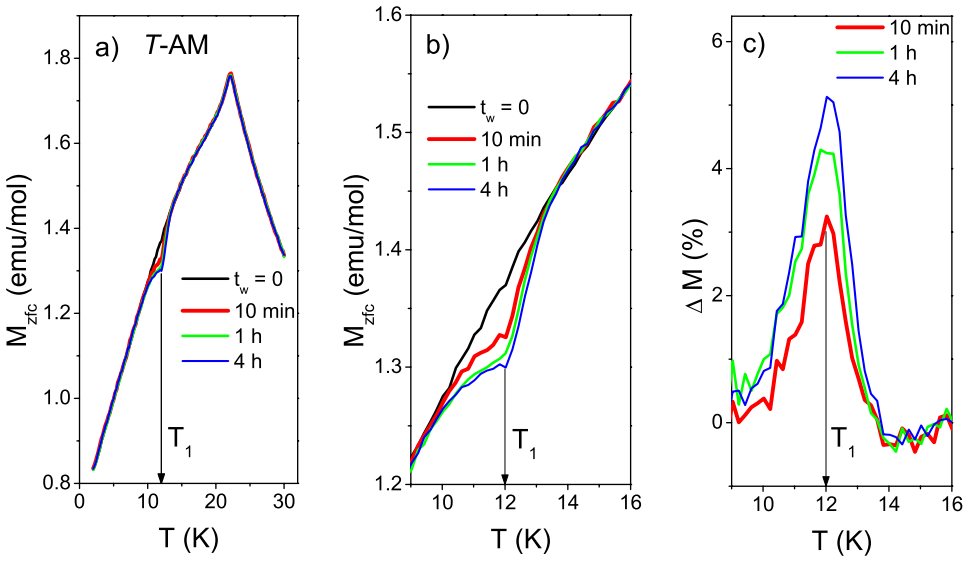

FIG. 9. (Color online) Memory effect in the T-AM sample. In (a), M_{zfc}'s obtained for different aging intervals t_w=0, 10 min, 1 h, and 4 h at T_1=12 K are shown. Expanded portions of the curves in the vicinity of T_1 are displayed in (b). ME is manifested as a drop of M_{zfc} of the aged curves with respect to the reference (unaged) curve $M_{zfc}(t_w=0)$ in the vicinity of the aging temperature T_1. In (c), the normalized difference between the reference curve and the curves with aging at T_1, $\Delta M=[M_{zfc}(t_w=0)-M_{zfc}(t_w)]/M_{zfc}(t_w=0)$, is shown.

identical to those of the T-AM sample, all showing consistently the ME effect regardless of the differences in the samples' composition and/or structure.

B. One stop at different temperatures

In order to find the dependence of the ME on the choice of the stop temperature T_1 within the nonergodic phase, we performed a set of experiments just described on the binary T-AM sample (T_f=22.0 K), where the cooling always began at the starting temperature 100 K and the sample was continuously cooled in zero field to different stop temperatures T_1=24, 22, 20, 18, 16, 14, 12, 10, 8, 6, 4, and 2 K, where the first temperature is slightly above T_f and the second is at T_f. In each run, aging at T_1 for a time t_w=1 h was employed and a reference run (t_w=0) was performed as well. The resulting M_{zfc}'s are displayed in Fig. 12(a), showing that the memory imprint is consistently observed at all temperatures below T_f, whereas the effect is absent at and above T_f, indicating that the ME does not extend outside the nonergodic phase. The normalized magnetization difference ΔM for all stop temperatures is shown superimposed in Fig. 12(b). On going below T_f, the amplitude of ΔM first increases for a decreasing stop temperature and exhibits a maximum at T_1=10 K. For $T_1<10$ K, ΔM decreases quite rapidly but remains nonzero down to the lowest investigated stop temperature T_1=2 K. This nonmonotonous behavior is clearly incompatible with the assumption of thermally activated motion (spin flipping) of one type of spins or clusters, which should freeze exponentially upon cooling.

The approach of ΔM toward saturation for $t_w\to\infty$ at different stop temperatures has been studied at T_1=18, 12, and 6 K, employing a set of eleven aging intervals t_w between 4 min and 4 h. ΔM amplitude as a function of t_w is shown in Fig. 12(c). The result is surprising: (i) for all three temperatures, the approach toward the saturated value $\Delta M(t_w\to\infty)$ proceeds with very similar time constant and (ii) majority of the ME imprint happens within the initial t_w interval of about 30 min, whereas t_w's longer than 1 h add very little to the effect. The dynamics of ME is thus astonishingly insensitive to the choice of T_1 (or, better, to the difference T_f-T_1). Such

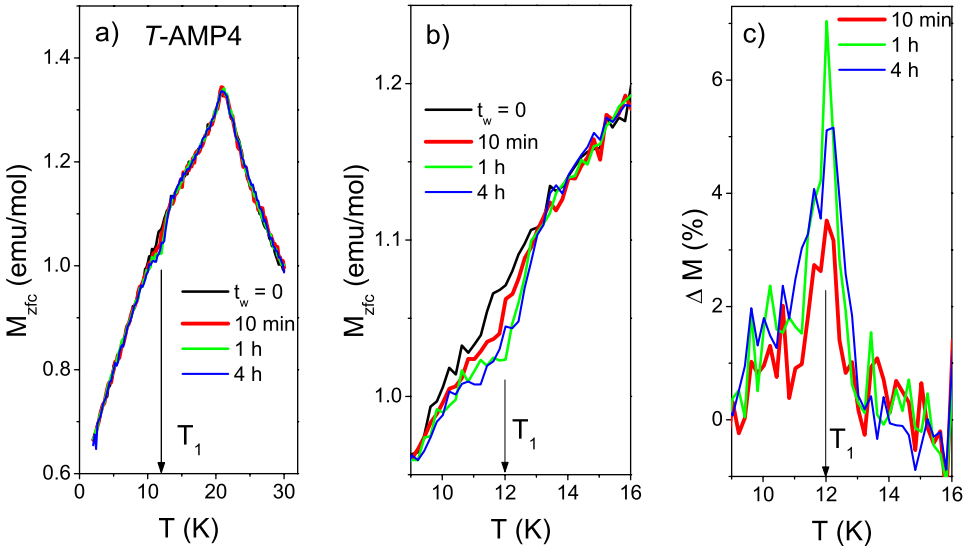

FIG. 10. (Color online) Memory effect in the T-AMP4 sample. The captions to panels (a), (b), and (c) are identical to those in Fig. 9. The apparently larger ΔM peak value of the t_w=1 h curve as compared to the 4 h curve in the panel (c) is fictitious and is a consequence of the large noise of the M_{zfc} curves of this sample.

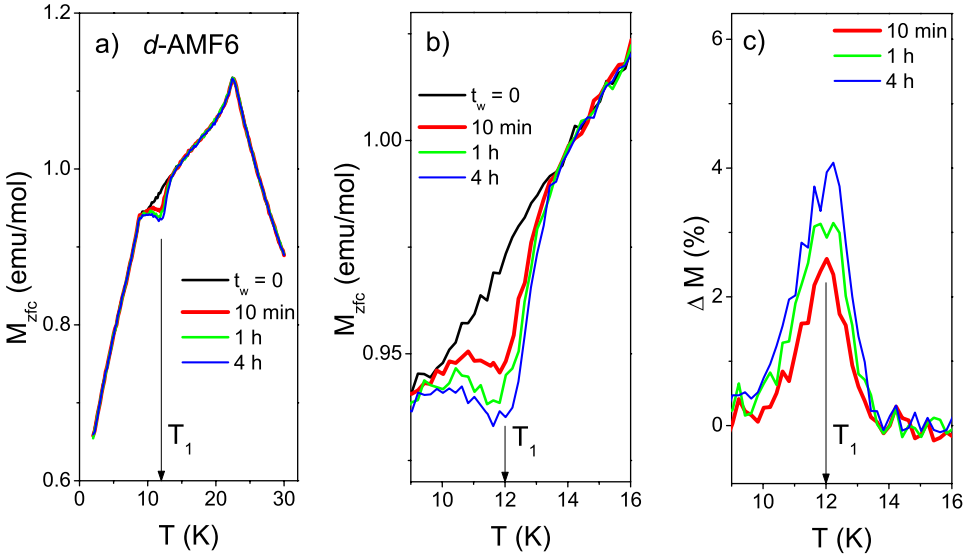

FIG. 11. (Color online) Memory effect in the *d*-AMF6 sample. The captions to panels (a), (b), and (c) are identical to those in Fig. 9.

behavior is in clear contrast to the thermally activated dynamics observed in conventional SGs,[6,21] whereas similar insensitivity of the aging effects on temperature was observed in the geometrically frustrated *kagomé* AFM[11] $(H_3O)Fe_3(SO_4)_2(OH)_6$. Currently, there is no simple explanation for this incredible insensitivity of the ME on the temperature.

C. Effect of starting temperature and reproducibility

The possible influence of the starting temperature on the ME was investigated on the *T*-AM sample by performing a set of experiments employing aging for t_w=1 h at T_1=12 K with the zfc cooling started at 100, 50, and 30 K. The resulting M_{zfc}'s are shown in Fig. 13, where the curves corresponding to different starting temperatures are indistinguishable, showing that the choice of the starting temperature anywhere within the ergodic phase above T_f has no influence on the ME. In order to check for the reproducibility of the measurements, the same set of experiments was repeated again just after the first set was completed. The curves of the second set are also shown in Fig. 13 and are indistinguishable from the first set. The ME is thus fully reproducible.

D. Two stops in one zero-field-cooled run

In the next set of experiments (performed on the *T*-AM sample), we have checked whether the spin system can memorize more than one stop (i.e., subsequent isothermal aging at more than one temperature) within the same zfc run. The starting temperature was 100 K and cooling was stopped twice, each time for t_w=1 h. The following pairs of stop temperatures were employed: 18 K+12 K, 18 K+10 K, 16 K+8 K, and 12 K+6 K. After the second stop, the cooling resumed to 2 K, where the magnetic field was applied and M_{zfc} was measured in a heating run. The results are displayed in Fig. 14(a), where it is observed that both stops have been memorized by the spin system. Moreover, the memory imprint in M_{zfc} at a given stop temperature is independent of the rest of the thermal history in one zfc run. This is evident from Fig. 14(b) where ΔM is plotted as a function of temperature for all two-stop runs. ΔM for the stop tem-

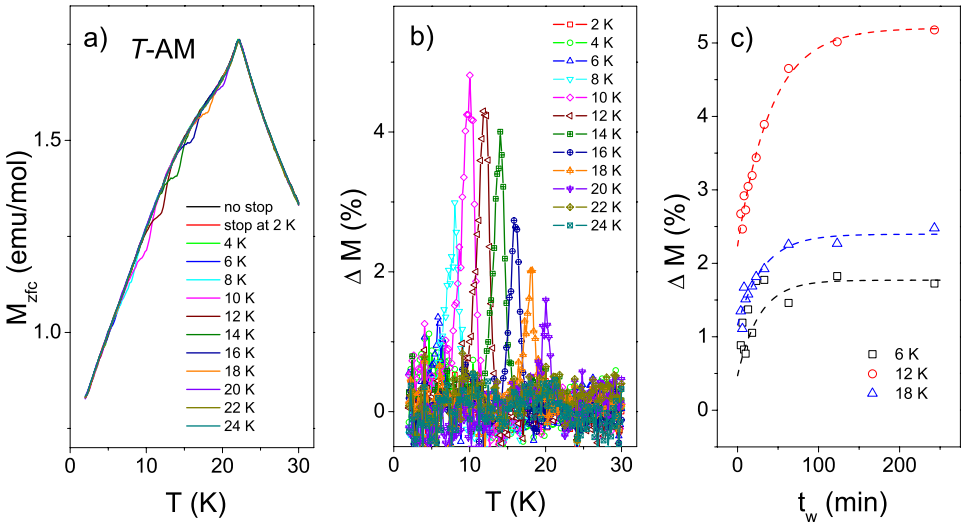

FIG. 12. (Color online) Memory effect in the *T*-AM sample (T_f=22.0 K) at different stop temperatures T_1=24, 22, 20, 18, 16, 14, 12, 10, 8, 6, 4, and 2 K, always employing the same aging interval t_w=1 h. In (a), M_{zfc}'s for all stop temperatures are shown superimposed. Panel (b) shows the normalized magnetization difference ΔM between the unaged and aged M_{zfc}'s for all stop temperatures. In (c), the approach of ΔM toward a saturated value as a function of t_w at the stop temperatures T_1=18, 12, and 6 K is shown. Dashed lines are guides for the eyes.

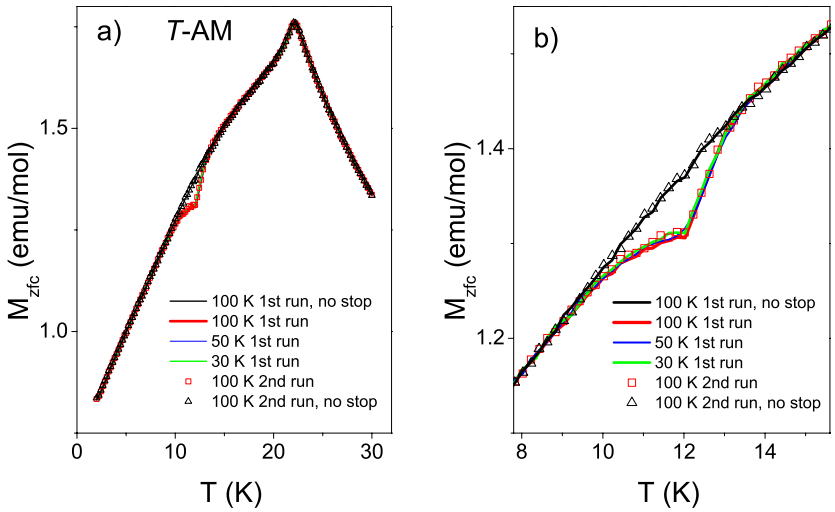

FIG. 13. (Color online) The effect of starting temperature for the zfc cooling on the ME in the *T*-AM sample and reproducibility of the results. M_{zfc}'s of a set of experiments employing aging for $t_w=1$ h at $T_1=12$ K with the zfc cooling started at 100, 50, and 30 K are shown superimposed as solid (online colored) lines. A reference run (black solid line) with no aging is also given. The same set of experiments was repeated again just after the first set was completed. The M_{zfc} curves of the second set (shown by symbols only) are also superimposed in the figure. The curves of the second set are indistinguishable from the first set.

perature 12 K is the same in the two runs with stop temperatures 18 K+12 K and 12 K+6 K.

The independence of the ME on the thermal history in one zfc run is also demonstrated in Fig. 14(c), where ΔM's for the two-stop runs 18 K+12 K and 12 K+6 K from Fig. 14(b) are plotted together with the ΔM's for one-stop runs 18, 12, and 6 K from Fig. 12(b) (in all experiments, the same $t_w=1$ h was employed at any stop temperature). We again find consistently that ΔM at a given stop temperature is independent of the rest of the thermal history in one zfc run (provided that no positive temperature steps are involved, to be discussed next).

E. Memory erase by a positive temperature cycle

The following set of experiments, performed on the *T*-AM sample, demonstrates that the memory imprint in M_{zfc} can be erased by a positive temperature cycle *within* the nonergodic phase. For clarity, the experiments are presented in triple-axis temperature-time-magnetization diagrams. In all

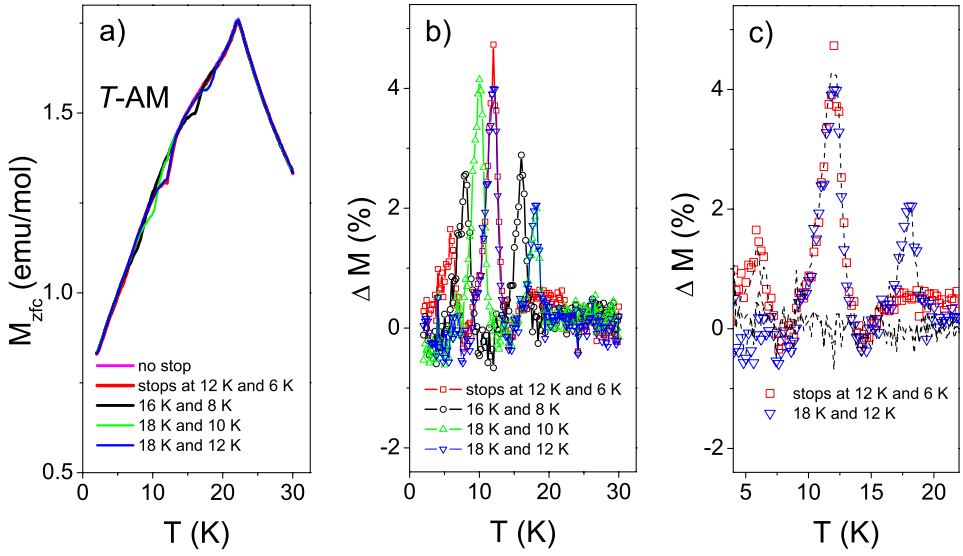

FIG. 14. (Color online) Two stops in one zfc run (experiments performed on the *T*-AM sample). In (a), M_{zfc}'s of four experiments, employing pairs of stop temperatures 18 K+12 K, 18 K+10 K, 16 K+8 K, and 12 K+6 K, are shown superimposed. At each stop temperature, aging for $t_w=1$ h was employed. Panel (b) shows ΔM as a function of temperature for all two-stop runs. In (c), ΔM's for the two-stop runs 18 K+12 K and 12 K+6 K (symbols only) from panel (b) are plotted together with the ΔM's for one-stop runs 18, 12, and 6 K (dashed curves) from Fig. 12(b) (in all experiments, the same $t_w=1$ h was employed at any stop temperature). The results show consistently that ΔM at a given stop temperature is independent of the rest of the thermal history in one zfc run.

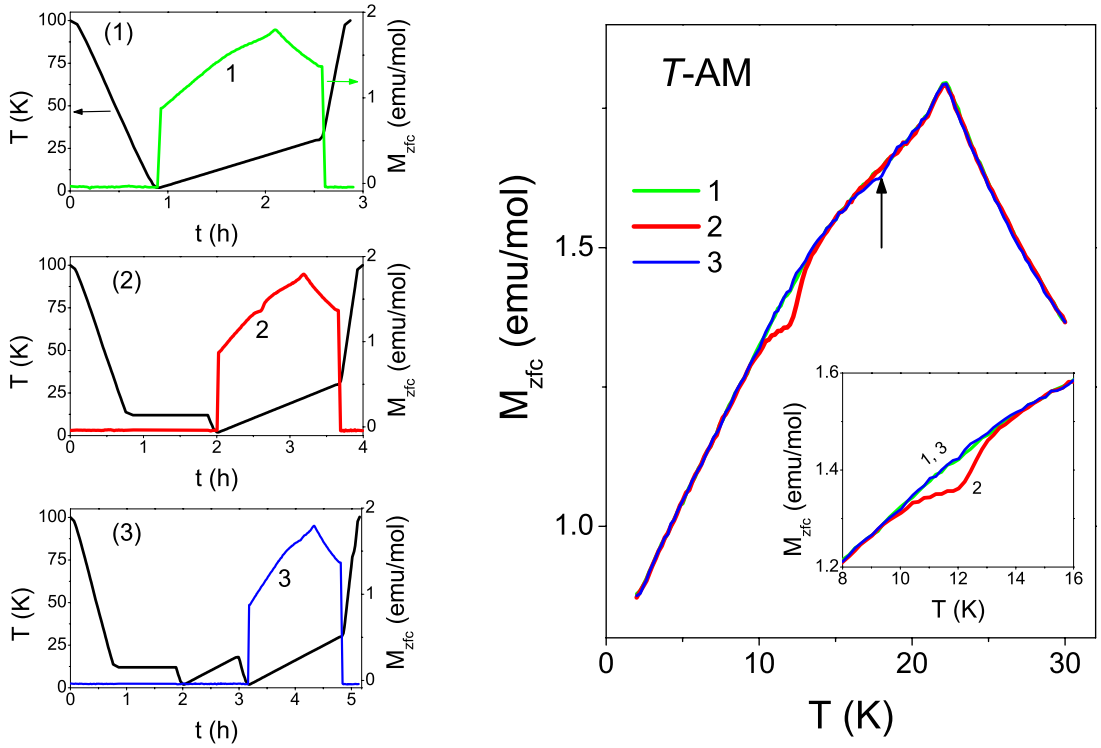

FIG. 15. (Color online) Memory erase by a positive temperature cycle within the nonergodic phase for the T-AM sample. Three experiments are presented: (1) the no-stop reference run (the corresponding M_{zfc} is labeled as the curve 1); (2) the simple one-stop run with aging for $t_w=1$ h at $T_1=12$ K (curve 2); (3) in the third experiment, the zfc run to 2 K was performed first with aging for $t_w=1$ h at $T_1=12$ K. In the next step, the sample was continuously heated to 18 K (that is still below $T_f=22.0$ K), where the heating was reversed to cooling back to 2 K, all in zero field. At 2 K, the field was applied and M_{zfc} (curve 3) was measured up to 30 K. The experiments are shown in triple-axis (temperature-time-magnetization) representation, where the black lines show the temperature-time profile and the colored curves are M_{zfc}'s. M_{zfc}'s of all three experiments are superimposed in the main panel, showing that the positive temperature cycle to 18 K has erased the memory. Small difference between curves 1 and 3 in the vicinity of 18 K (indicated by an arrow) is due to the fact that some time was needed to reverse the direction of the temperature change after the positive temperature step, so that some aging took place at 18 K.

experiments, zero field cooling started at 100 K.

The first set of experiments consisted of three experiments (Fig. 15): (1) the no-stop reference run; (2) the simple one-stop run with aging for $t_w=1$ h at $T_1=12$ K; (3) in the third experiment, the zfc run to 2 K was first performed with aging for $t_w=1$ h at $T_1=12$ K. In the next step, the sample was continuously heated to 18 K (that is still below $T_f=22.0$ K), where the heating was reversed to cooling back to 2 K, all in zero field. There, the field was applied and M_{zfc} was measured up to 30 K. The M_{zfc}'s of the three experiments are shown superimposed in the main panel of Fig. 15, where we observe that the positive temperature cycle to 18 K has erased the memory imprint.

In order to check whether the small magnetic field applied during the positive temperature step to 18 K has any effect on the memory erase, we performed an additional experiment similar to that with the positive temperature cycle just described [experiment (3)], but this time with the field switched on during heating to 18 K (Fig. 16). We observe that the memory is erased as well, so that the small magnetic field during the positive temperature cycle has no effect on the memory erase.

The memory erase by a small positive temperature cycle is also evident from the following additional experiment (Fig. 17). The sample was zero field cooled to 12 K, where aging for $t_w=1$ h was employed. The sample was then heated to 15 K (again in zero field) and then cooled continuously to 2 K, where the field was applied and M_{zfc} was measured. Comparison to the reference run shows that the memory imprint at 12 K was completely erased also by this positive temperature cycle.

F. Memorizing again after the memory erase by a positive temperature cycle

The above experiments show that a positive temperature cycle within the nonergodic phase erases the memory. It is interesting to see whether aging at a given temperature just after the memory was erased can be memorized again by the spin system. For this purpose, we have conducted the following experiments: (1) a simple one-stop run with $t_w=1$ h at $T_1=12$ K and (2) an experiment employing first the zfc run to 2 K with aging for $t_w=1$ h at $T_1=12$ K. At 2 K, the field was applied and the measurement of M_{zfc} was performed in a heating run up to 18 K, where the heating was stopped, the field was removed, and zero field cooling was performed back to 2 K with additional stop for $t_w=1$ h at $T_1=12$ K. At 2 K, the field was reapplied and M_{zfc} was measured up to 30 K; (3) the same experiment, but the field was not applied during heating to 18 K. We observe (Fig. 18) that the

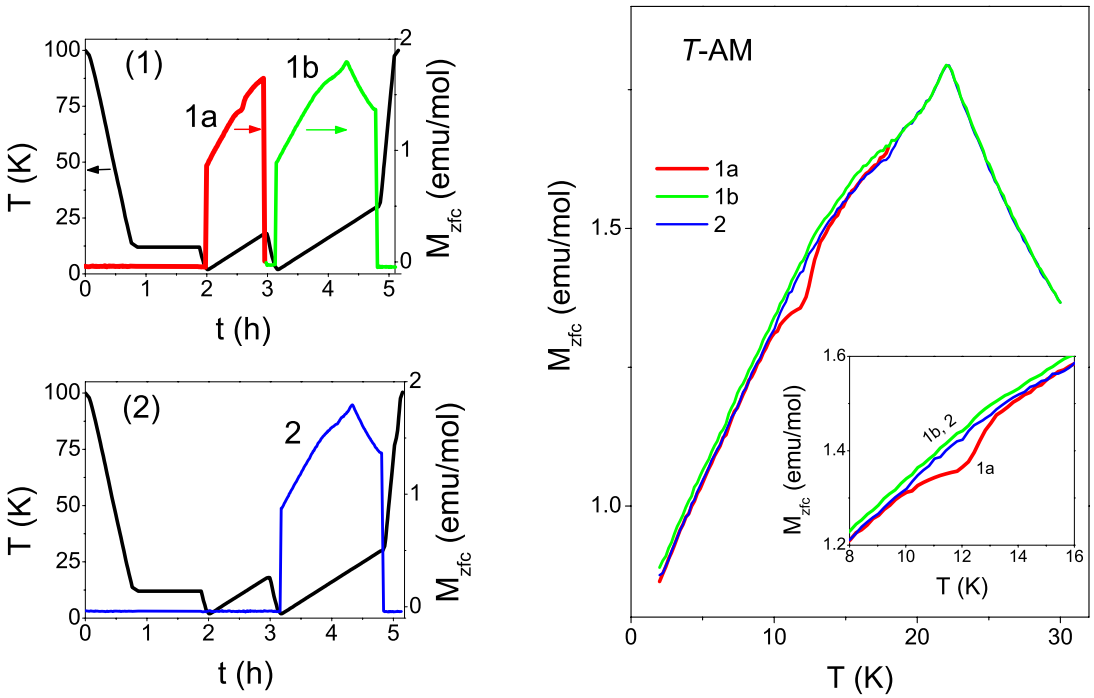

FIG. 16. (Color online) The influence of small magnetic field applied during the positive temperature step on the memory erase (for the *T*-AM sample). Two otherwise identical experiments with aging at $T_1=12$ K for $t_w=1$ h during the initial zfc run were performed, followed by a positive temperature step to 18 K, where in experiment (1), small magnetic field was applied during the positive step and M_{zfc} (curve 1a) was measured, whereas in experiment (2), the field was switched off during the positive step. M_{zfc}'s measured after the positive step (curves 1b and 2) both show complete memory erase (see the main panel), demonstrating that the small magnetic field during the positive step has no influence on the erase.

memory imprint in M_{zfc} is consistently observed for all three experiments. The M_{zfc} curves of the simple one-stop run and the experiment without the field during heating to 18 K are indistinguishable, whereas M_{zfc} of the experiment with the field on during heating to 18 K is slightly larger, but with the same memory imprint as in the other two cases. The spin system is thus ready to memorize again just after the memory was erased and low external magnetic field has no influence on this phenomenon.

G. Contribution of aging at lower temperature to aging at higher temperature

It is interesting to see whether aging at a lower temperature has any influence on the aging at a higher temperature. We performed two experiments: (1) a simple one-stop run with $t_w=4$ h at $T_1=12$ K and (2) an experiment where the zfc cooling was first stopped at 12 K for $t_{w1}=1$ h. The sample was then cooled to $T_2=10$ K, where aging for $t_{w2}=1$ h was employed. The temperature was then raised back to $T_1=12$ K, where additional aging for a time $t_{w3}=3$ h was employed before the cooling resumed to 2 K. There, the field was applied and M_{zfc} was measured. The total aging time spent at 12 K, $t_{w1}+t_{w3}=4$ h, was therefore the same as in the first experiment, but there was additional aging for $t_{w2}=1$ h at 10 K. Figure 19 shows that M_{zfc}'s of the two experiments are indistinguishable, showing identical memory imprint at 12 K but no imprint at 10 K. Positive temperature step from 10 to 12 K has obviously erased aging at 10 K. Hence, aging at a lower temperature does not contribute to aging at a higher temperature; the effect of low-temperature aging is erased by the positive temperature step. Any (large enough) positive temperature step thus rejuvenates the system.

H. Summary of the memory effect experimental results

The above experimental results on the ME and rejuvenation can be summarized as follows:

(i) A nonergodic magnetically frustrated spin system memorizes its thermal history in a zero-field-cooled run. It memorizes both the temperature where the cooling was temporarily stopped and for how long it was stopped. Though the ME is a result of an out-of-equilibrium spin dynamics, it is a fully reproducible phenomenon.

(ii) Isothermal aging of the spin system is inscripted in the zero-field-cooled electronic magnetization M_{zfc}. The inscription appears as diminution (a dip) in M_{zfc} with respect to M_{zfc} of the unaged system. Though M_{zfc} is a magnetic quantity, the memory inscription is thermally induced and happens in the absence of any external magnetic field during cooling in zero field.

(iii) Although aging is performed at a sharp temperature, the normalized difference ΔM of the zfc magnetizations of the aged and unaged systems is smeared over a finite temperature interval about ± 2 K around the stop temperature. Within this interval, ΔM shows a resonant character, being peaked at the aging temperature. For the longest aging time employed in our experiments, $t_w=4$ h, ΔM amounts up to

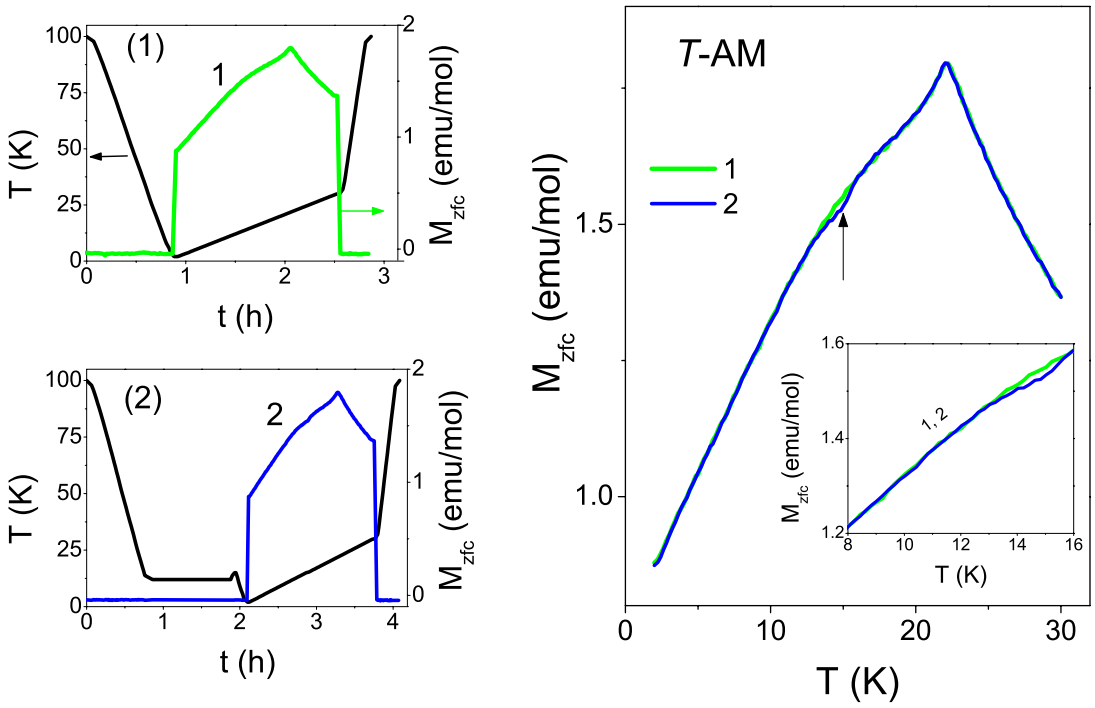

FIG. 17. (Color online) Memory erase by a small positive temperature cycle for the *T*-AM sample. The sample was zero field cooled to 12 K, where aging for $t_w=1$ h was employed. After aging, the sample was heated to 15 K in the absence of external magnetic field and then cooled continuously to 2K, where the field was applied and M_{zfc} was measured (curve 2). Comparison to the reference (no-stop) run (curve 1) shows that the memory was completely erased also by this positive temperature cycle. Small difference in the vicinity of 15 K (indicated by an arrow) is due to the fact that some time was needed to reverse the direction of the temperature change after the positive temperature step, so that some aging took place.

5% (depending on the choice of the stop temperature).

(iv) The ME is consistently observed at any stop temperature below T_f but does not extend outside the nonergodic phase. Experiments performed on the *T*-AM sample ($T_f=22.0$ K), employing the same aging interval $t_w=1$ h at all stop temperatures, show that ΔM as a function of the stop temperature exhibits unexpected behavior. ΔM first increases for a decreasing stop temperature from T_f to 10 K, where it exhibits a maximum. For the stop temperatures below 10 K, ΔM decreases but remains nonzero down to the lowest investigated stop temperature of 2 K.

(v) At any investigated stop temperature, majority of the memory imprint happens during the initial aging interval of $t_w \approx 30$ min. Longer aging up to 4 h adds little to the memory imprint. The approach of ΔM toward a saturated value upon $t_w \to \infty$ is astonishingly insensitive to the choice of T_1 (hence to the difference $T_f - T_1$), suggesting that the ME depends on temperature very weakly.

(vi) The choice of the starting temperature for the zero field cooling within the ergodic paraphase has no influence on the ME.

(vii) The spin system can memorize more than one stop in a single zero-field-cooled run. Isothermal aging at a given temperature is independent of the rest of the thermal history in the same zfc run (provided that no positive temperature steps are involved).

(viii) A positive temperature cycle *within* the nonergodic phase completely erases the memory and hence rejuvenates the spin system. M_{zfc} measured in a zfc experiment after a positive temperature cycle is again that of the young (unaged) system with no memory imprint. Memory is erased thermally, regardless of the presence or absence of a small magnetic field. Any heating above T_f into the ergodic phase erases the memory as well. This is different from canonical SGs, where correlated spin clusters extend far into the ergodic phase, so that heating to temperatures as high as $10T_f$ is needed to fully reset the ME.

(ix) The spin system is ready to memorize isothermal aging again just after the memory has been erased by a positive temperature cycle within the nonergodic phase. Memory erase has no effect on the subsequent memory imprint (as the positive temperature cycle has completely removed the effect of previous aging). Low external magnetic field has no influence on this phenomenon.

(x) Aging at a lower temperature does not contribute to aging at a higher temperature; the effect of low-temperature aging is erased by the positive temperature step.

VI. DISCUSSION

In order to understand the microscopic origin of the ME in the investigated *T*-phase and decagonal samples, let us first discuss specific features of the spin system in these compounds, as derived from the magnetic measurements. The analysis of the Curie constants (Table I) reveals that the average magnetic moment per magnetic ion $\bar{\mu}_{eff}=2.7\mu_B$ in all samples is reduced by a factor of about 2 with respect to the values expected for the bare Mn and Fe ions in an insulating

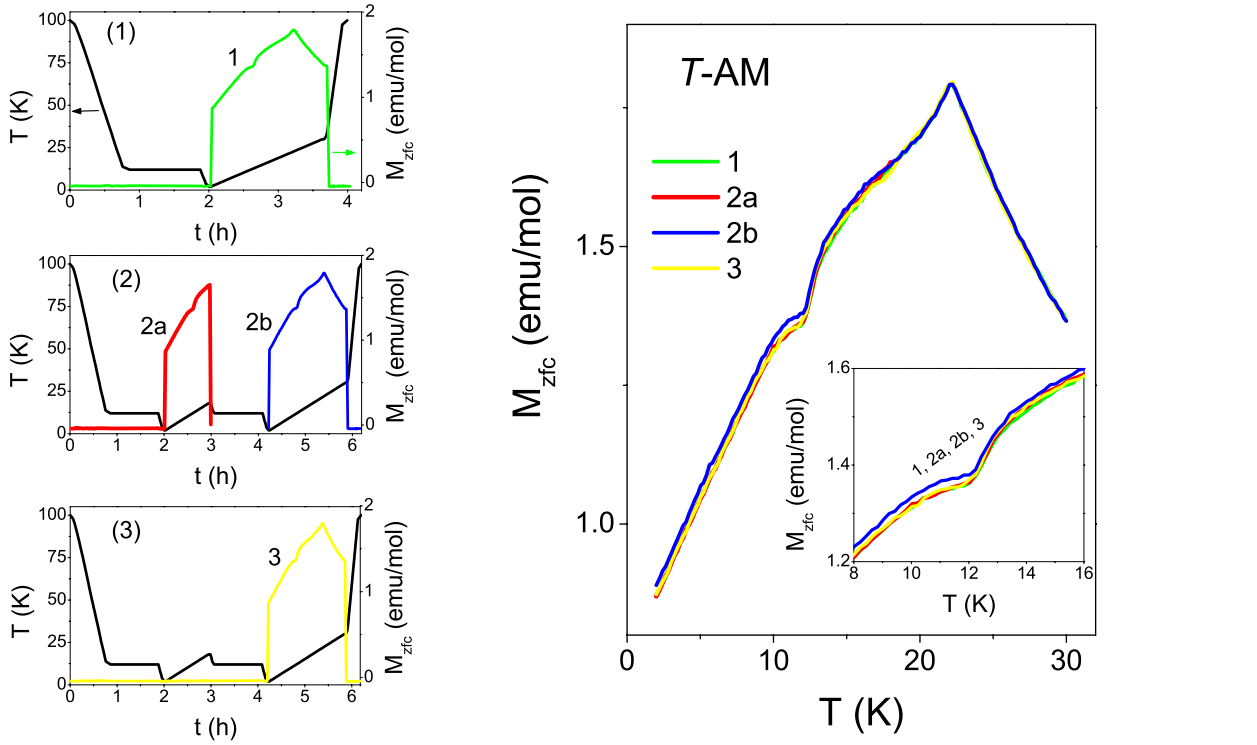

FIG. 18. (Color online) Memorizing again just after the memory was erased by a positive temperature cycle (for the *T*-AM sample). Three experiments were conducted: (1) a simple one-stop run with t_w=1 h at T_1=12 K (curve 1) and (2) an experiment employing first the zfc run to 2 K with aging for t_w=1 h at T_1=12 K. At 2 K, the field was applied and the measurement of M_{zfc} (curve 2a) was performed in a heating run up to 18 K, where the heating was stopped, the field was removed and zero field cooling was performed back to 2 K with additional stop for t_w=1 h at T_1=12 K. At 2 K, the field was reapplied and M_{zfc} (curve 2b) was measured up to 30 K; (3) the same experiment, but the field was not applied during heating to 18 K (curve 3). M_{zfc}'s are superimposed in the main panel, all showing the memory imprint.

environment. This difference can be attributed to the electrically conducting state of the investigated phases, where the ions are "dressed" by a conduction-electron cloud that partially compensates their spin. The degree of spin compensation depends on the local conduction-electron density of states at the sites of the magnetic Mn and Fe atoms and generally varies from site to site. The distribution of magnetic moments over the lattice sites was determined theoretically for the Hiraga model of the binary T-Al_3Mn phase (more precisely, for one of its realizations, as fractional occupations of the lattice sites were replaced by integer values, either 0 or 1) by using spin-polarized *ab initio* calculations.[32] The results show that two of the Mn sites [Mn(5) and Mn(6)] carry substantial magnetic moments (0.66 and 1.0 μ_B, respectively) and there is also a small moment at the Mn(2) site, whereas all other Mn sites carry moments smaller than 0.1 μ_B (positive or negative). Though the average effective moments per magnetic ion in our samples are significantly larger than this prediction, the *ab initio* calculations offer the following qualitative picture: there exists a distribution of partially compensated magnetic moments at different Mn and Fe sites, ranging from large, of the order of a μ_B, to small moments of a fraction of a μ_B.

The next important feature is the coupling between the moments. Paramagnetic susceptibilities yielded negative Curie–Weiss temperatures θ, suggesting dominant AFM-type coupling that favors antiparallel spin alignment. The exact nature of the exchange coupling (either direct exchange or Ruderman–Kittel–Kasuya-Yosida exchange) is not clear. The experiments reveal that the couplings are distributed in magnitude from weak to strong. This is evident from the magnetic field dependence of the zfc and fc susceptibilities shown in Fig. 2(a), where increasing magnetic field polarizes the spins, so that the difference between χ_{zfc} and χ_{fc} diminishes (the zfc-fc splitting is shifted to lower temperatures) and the polarized system behaves paramagneticlike. A continuous disappearance of the difference between χ_{zfc} and χ_{fc} upon increasing the field up to 50 kOe reflects a continuous distribution of the exchange coupling energies. The strongest exchange-coupled spins are not polarized even by the field as large as 50 kOe [as evident from the remaining zfc-fc susceptibility splitting of the 50 kOe curves, shown in the inset of Fig. 2(a)].

The exchange-coupled spins are in a frustrated configuration to each other, resulting in broken ergodicity below T_f. The dynamics of the nonergodic phase is associated with progressive freezing of spin orientations (where, instead of single spins, one can also consider cluster spins). Upon cooling below T_f, the strongest coupled spins freeze first, whereas less coupled spins freeze at lower temperatures, once k_BT becomes smaller than the energy needed to reverse a spin. A continuous distribution of couplings implies that at any temperature within the nonergodic phase, some spins just freeze, stronger-coupled spins are already frozen (they

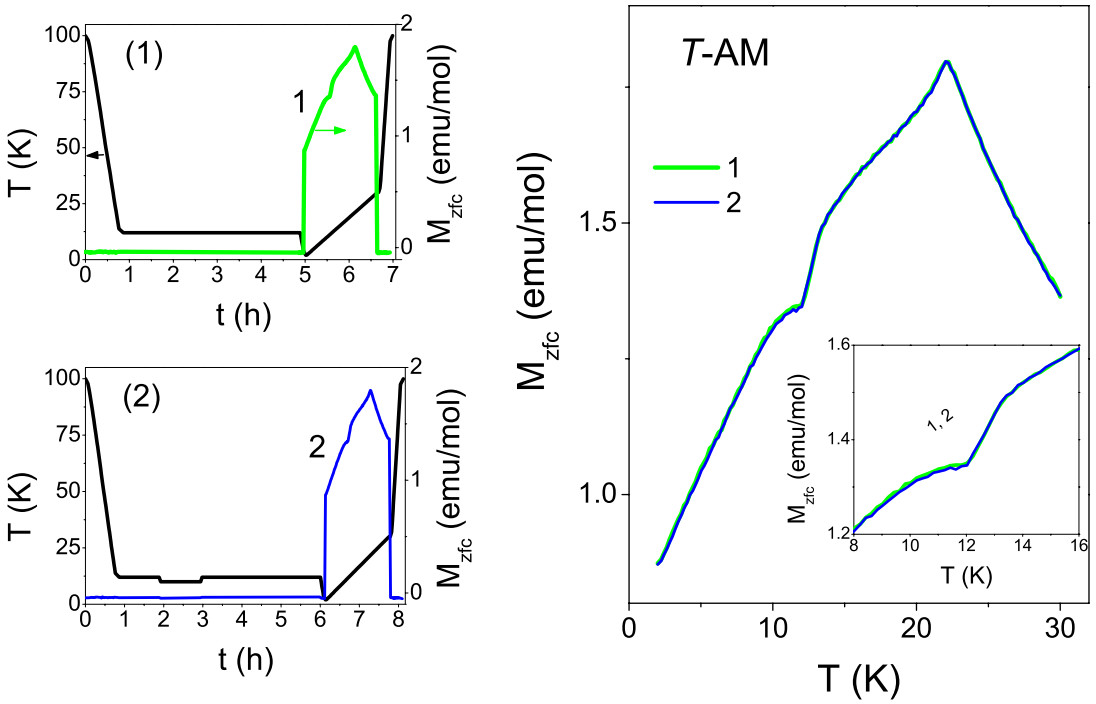

FIG. 19. (Color online) Contribution of aging at lower temperature to aging at higher temperature (for the T-AM sample). Two experiments were performed: (1) a simple one-stop run with $t_w=4$ h at $T_1=12$ K (curve 1) and (2) an experiment where the zfc cooling was first stopped at 12 K for $t_{w1}=1$ h. The sample was then cooled to $T_2=10$ K, where aging for $t_{w2}=1$ h was employed. The temperature was then raised back to $T_1=12$ K, where additional aging for a time $t_{w3}=3$ h was employed, before the cooling resumed to 2 K. There, the field was applied and M_{zfc} (curve 2) was measured. The total aging time of 4 h spent at 12 K was the same in both experiments, but there was additional aging for $t_{w2}=1$ h at 10 K in the second experiment. M_{zfc}'s of the two experiments, shown superimposed in the main panel, are indistinguishable.

froze at a higher temperature) and some are still thermally reorienting and will freeze at a lower temperature. This real-space picture can be translated into the phase-space picture.[6,21] A real-space spin reorientation changes the spin configuration from one to another metastable state, which in the phase space means jump of the system from one to another minimum in the highly degenerate free-energy landscape. The difference in the exchange energy upon spin reversal represents the energy barrier in the phase space that should be surmounted by the spin system to jump from one to another minimum. A distribution of exchange energies is related to a distribution of energy barriers. In the phase-space representation, aging during t_w at T_1 can be viewed as a random walk between the minima of the free energy[13,21,22] [Fig. 5(b)] by jumping over the barriers that are of the order k_BT_1 or smaller.

In order to understand the aging-induced thermal imprint (a dip) in M_{zfc}, we discuss first the specific temperature dependence of the reference (no-aging) M_{zfc}, which exhibits a continuous increase toward T_f upon heating and a cusp at T_f. In the first part of the zfc experiment, the spin system is cooled in zero field from the paraphase through T_f down to the lowest temperature. During continuous cooling, the nonergodic spin system has no time to equilibrate at any temperature in an energetically favorable configuration, not even locally. At the lowest temperature, all spins are randomly frozen in a spin-glass configuration with no net spontaneous magnetization [Fig. 20(a)]. This configuration is metastable and frustrated spins can easily be reoriented by thermal energy k_BT. In a subsequent measurement of M_{fc}, a small field is applied at the lowest temperature and the system is continuously heated. The nonzero M_{zfc} is now originating from those spins that have thermally reoriented into the field in order to minimize their Zeeman energy. Due to the increase of the thermal energy upon heating, spins with increasingly stronger exchange couplings reorient into the field, resulting in a progressive buildup of M_{zfc} toward T_f until at T_f, M_{zfc}

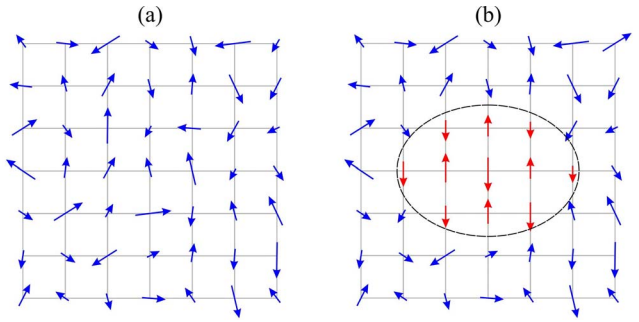

FIG. 20. (Color online) (a) Schematic representation of a randomly frozen spin-glass configuration with no net spontaneous magnetization, obtained in a continuous cooling run. (b) During isothermal aging period, some spins quasiequilibrate locally into more stable configurations (online red-colored spins within the dashed region, assuming an AFM-type coupling) and form ordered spin droplets.

reaches the full equilibrium magnetization of the system for that particular temperature. Above T_f, the ergodic spin system behaves Curie-like paramagnetically that results in a cusp at T_f and a $1/T$-type decrease of the magnetization toward higher temperature.

The ME and rejuvenation in a zfc experiment with aging for a time t_w at T_1 can be understood as follows. During isothermal aging at T_1, the spins that are still mobile at that temperature try to equilibrate in an energetically favorable configuration among themselves and with the spins already frozen. In this way, localized quasiequilibrated "spin droplets" are formed. Due to the predominant AFM-type coupling, the magnetization of the droplets tends to zero. Magnetically quasiordered spin droplets are in a more stable configuration than the rest of the spin-glass matrix, so that higher thermal energy is needed to reverse a spin within a droplet. Resuming continuous zero field cooling after the isothermal aging, magnetic order within the droplets is partially frozen [it is frozen for those spins whose energy to reverse a spin is about k_BT_1, whereas weaker-coupled (more reorientable) spins are still mobile and gradually freeze in a spin-glass configuration at lower temperature]. At the lowest temperature of the zfc run with aging at T_1, all spins with reorientational energies either larger or smaller than k_BT_1 are in a spin-glass configuration, whereas the spins with energies of about k_BT_1 form regions with more stable quasiequilibrated configurations [Fig. 20(b)]. Upon M_{zfc} measurement in a subsequent heating run, M_{zfc} builds up as in the no-aging case, except in the vicinity of T_1, where now higher thermal energy is needed to reorient the spins in the more stable quasiordered droplets. Consequently, M_{zfc} shows diminution at T_1 relative to the no-aging case. The fact that spins in the droplets are only slightly stronger coupled than those in the spin-glass configuration is evident from the fact that rejuvenation (the point where M_{zfc}'s of the aging and no-aging cases upon heating match again) appears at only slightly higher temperature than T_1. In our experiments, this happens about $\Delta T \approx 2$ K above. Memory erase (rejuvenation) involves destroying the more stable magnetic order within the quasiequilibrated droplets by thermal reorientations. For this to happen, the positive temperature step should be large enough that the thermal energy can overcome the exchange-energy barriers for the spin reorientations within the droplets. Figures. 9–11 suggest that the positive temperature step of about $\Delta T \approx 2$ K is sufficient to completely rejuvenate the system.

The above qualitative picture consistently explains all the experimentally observed features of the ME and rejuvenation, as presented in items (i) to (x) of Sec. V H of the ME experimental results given in the previous chapter. The gradual freezing of spins throughout the nonergodic phase due to distributed reorientational energies explains why aging at more than one temperature upon zfc cooling can be memorized. It also explains the apparent weak temperature dependence of the ME: though spin dynamics is thermally activated, the distribution of jump barriers implies that different spins freeze over the entire nonergodic phase. The fact that the normalized difference ΔM between the zfc magnetizations of the aged and unaged systems at any stop temperature shows resonant character is a consequence of the energy conservation; only those spins attain quasiequilibrated configurations at T_1 by thermal flipping whose "up-down" energy difference matches k_BT_1. The magnitude of ΔM at a particular stop temperature is a measure of the fraction of spins in the ordered droplets relative to the total number of spins. In our investigated systems, this fraction amounts up to 5%, depending on the stop temperature. The unusual temperature dependence of ΔM as a function of the stop temperature shown in Fig. 12(b) reflects the size of the droplet fraction relative to the total size of the magnetic phase at different stop temperatures and hence provides indirect information on the distribution of energy barriers for the spin reorientations.

The above picture of quasiequilibrated droplets that form locally during isothermal aging and are in a more stable configuration than the rest of the SG matrix also explains the TRM-decay experiments. In the TRM field-cooled run, the ordered droplets form during the t_w aging interval in a field H_{fc}, where the spin system approaches an equilibrium state with nonzero magnetization M_{fc} in a field H_{fc}. The attained spin order corresponds to the $M_{fc} \neq 0$ state and is thus different from the zero-magnetization order in the droplets that form in the ME experiments in zero field. The slow buildup of the TRM in H_{fc} during t_w, shown in the inset in Fig. 7(a), reflects the formation of quasiequilibrated droplets in the field. Specification of the equilibrium state in the applied $H_{fc} \neq 0$ is difficult, as the Zeeman and exchange interactions both affect the spin system to a similar extent. After the field is cut to zero, the equilibrium state with $M_{fc} \neq 0$ in H_{fc} is replaced by a state with zero magnetization in $H_{fc}=0$ and the spin system proceeds toward this state during the decay time t. Quasiequilibrated spin order with $M_{fc} \neq 0$ in the droplets is more rigid than that in the SG matrix, so that more time is needed to destroy it toward the $M_{fc}=0$ state, which accounts for an increasing TRM amplitude and its slower decay in t upon increasing aging time t_w (Fig. 7). The H_{fc} dependence of the TRM magnitude can also be explained by this picture. Magnetic field "holds" the exchange-coupled spins (the jump barriers between metastable states are increased by the Zeeman energy, $M_{fc}H_{fc}$), which are less free to reorient, so that the approach toward quasiequilibrium during t_w in $H_{fc} \neq 0$ is slower in larger field, resulting in smaller TRM upon increasing H_{fc}. This is indeed observed in Fig. 8.

VII. CONCLUSIONS

The investigated Taylor-phase binary complex intermetallic compound T-Al_3Mn, its solid solutions with Pd and Fe, and its decagonal QC counterpart show pronounced broken-ergodicity magnetic phenomena (zfc-fc susceptibility splitting in low magnetic fields, frequency-dependent cusp in the ac susceptibility, hysteresis and remanence, ultraslow decay of the thermoremanent magnetization, and the memory effect and rejuvenation) associated with the out-of-equilibrium dynamics of a frustrated spin system. All these phenomena originate from the nonergodicity of a frustrated system of coupled spins that cannot come into thermal equilibrium on any accessible experimental time scale. At any temperature within the nonergodic phase, the spin system evolves toward

a global equilibrium, but since equilibration requires macroscopic times, we observe experimentally only transient effect of partial equilibration of localized domains. The degree of quasiequilibration depends on the time the spin system spends at a given temperature under steady external conditions, the phenomenon called aging. The most spectacular manifestations of the nonequilibrium dynamics are the ME, where a given state of the spin system attained during isothermal aging can be retrieved after a negative temperature cycle, and rejuvenation, where the memory is erased by a positive cycle. These two phenomena get simple explanation by considering that during isothermal aging, localized spin regions equilibrate into more stable configurations, so that higher thermal energy is needed to destroy these regions by spin flipping, as compared to the thermal energy required to reverse a frustrated spin in a disordered spin-glass configuration that forms in the case of no aging. This simple picture consistently explains all the observed experimental features of the ME and the aging effects in the TRM ultraslow decay, as elaborated in detail in this paper.

The observed aging phenomena are a consequence of the out-of-equilibrium dynamics of a nonergodic system and are not present in ergodic (thermal equilibrium) systems. Their common denominator is the slow approach toward equilibrium, which can globally never be reached. Such nonequilibrium dynamics is difficult to treat theoretically, as the relevant physical quantities are time dependent instead of being time-independent thermodynamic quantities. Among the magnetically frustrated spin systems, these phenomena have been observed before[1–5] in site-disordered spin glasses and geometrically frustrated site-ordered spin systems, but it is somewhat surprising that they also exist in the investigated T-phase Al_3Mn, $Al_3(Mn,Pd)$, and $Al_3(Mn,Fe)$ complex intermetallics and in the $Al_3(Mn,Fe)$ decagonal QC. Though substitutional site disorder may be expected for the solid solutions T-$Al_3(Mn,Pd)$ and T-$Al_3(Mn,Fe)$, it is not present in the binary T-Al_3Mn (apart from the ever-present chemical disorder on the lattice). There is also no indication that these systems belong to the class of geometrically frustrated spin systems. One reason for the frustration of the spin system in the T phases is perhaps the fact that magnetic moments at the transition-metal lattice sites are distributed in magnitude due to the site-dependent partial spin compensation by the conduction-electron cloud, which induces a distribution of exchange energies needed for frustration. Chemical disorder and geometrical frustration—though seemingly not of prime importance—may add to this effect as well.

ACKNOWLEDGMENT

This work was done within the activities of the 6th Framework EU Network of Excellence "Complex Metallic Alloys" (Contract No. NMP3-CT-2005-500140).

[1] J.-P. Bouchaud, L. F. Cugliandolo, J. Kurchan, and M. Mézard, in *Spin Glasses and Random Fields*, edited by A. P. Young (World Scientific, Singapore, 1998), pp. 161–224.
[2] N. Kawashima and H. Rieger, in *Frustrated Spin Systems*, edited by H. T. Diep (World Scientific, Singapore, 2004), pp. 491–586.
[3] E. Vincent, J. Hammann, M. Ocio, J.-P. Bouchaud, and L. F. Cugliandolo, in *Complex Behaviour of Glassy Systems*, Lecture Notes in Physics Vol. 492, edited by M. Rubi (Springer-Verlag, Berlin, 1997), pp. 184–219.
[4] P. Nordblad and P. Svedlindh, *Spin Glasses and Random Fields* (Ref. 1), pp. 1–28.
[5] J.-P. Bouchaud, V. Dupuis, J. Hammann, and E. Vincent, Phys. Rev. B **65**, 024439 (2001).
[6] See, for a review, K. Binder and A. P. Young, Rev. Mod. Phys. **58**, 801 (1986), and references therein.
[7] B. D. Gaulin, J. N. Reimers, T. E. Mason, J. E. Greedan, and Z. Tun, Phys. Rev. Lett. **69**, 3244 (1992).
[8] A. Lafond, A. Meerschaut, J. Rouxel, J. L. Tholence, and A. Sulpice, Phys. Rev. B **52**, 1112 (1995).
[9] P. Schiffer, A. P. Ramirez, D. A. Huse, P. L. Gammel, U. Yaron, D. J. Bishop, and A. J. Valentino, Phys. Rev. Lett. **74**, 2379 (1995).
[10] M. J. P. Gingras, C. V. Stager, N. P. Raju, B. D. Gaulin, and J. E. Greedan, Phys. Rev. Lett. **78**, 947 (1997).
[11] A. S. Wills, V. Dupuis, E. Vincent, J. Hammann, and R. Calemczuk, Phys. Rev. B **62**, R9264 (2000).
[12] J. Dolinšek, Z. Jagličić, M. A. Chernikov, I. R. Fisher, and P. C. Canfield, Phys. Rev. B **64**, 224209 (2001).
[13] J. Dolinšek, Z. Jagličić, T. J. Sato, J. Q. Guo, and A. P. Tsai, J. Phys.: Condens. Matter **15**, 7981 (2003).
[14] M. A. Taylor, Acta Crystallogr. **14**, 84 (1961).
[15] S. Balanetskyy, G. Meisterernst, M. Heggen, and M. Feuerbacher, Intermetallics **16**, 71 (2008).
[16] K. Hiraga, M. Kaneko, Y. Matsuo, and S. Hashimoto, Philos. Mag. B **67**, 193 (1993).
[17] H. Klein, M. Boudard, M. Audier, M. de Boissieu, H. Vincent, L. Beraha, and M. Duneau, Philos. Mag. Lett. **75**, 197 (1997).
[18] F. Hippert, V. Simonet, G. Trambly de Laissardière, M. Audier, and Y. Calvayrac, J. Phys.: Condens. Matter **11**, 10419 (1999).
[19] F. E. Mabbs and D. J. Machin, *Magnetism and Transition Metal Complexes* (Chapman and Hall, London, 1973), p. 7.
[20] J. A. Mydosh, *Spin Glasses: An Experimental Introduction* (Taylor & Francis, London, 1993), p. 67.
[21] M. Lederman, R. Orbach, J. M. Hammann, M. Ocio, and E. Vincent, Phys. Rev. B **44**, 7403 (1991).
[22] D. Chu, G. G. Kenning, and R. Orbach, Philos. Mag. B **71**, 479 (1995).
[23] K. Jonason, E. Vincent, J. Hammann, J. P. Bouchaud, and P. Nordblad, Phys. Rev. Lett. **81**, 3243 (1998).
[24] V. Dupuis, E. Vincent, J. P. Bouchaud, J. Hammann, A. Ito, and H. A. Katori, Phys. Rev. B **64**, 174204 (2001).
[25] P. Jönsson, M. F. Hansen, and P. Nordblad, Phys. Rev. B **61**, 1261 (2000).
[26] O. Cador, F. Grasset, H. Haneda, and J. Etourneau, J. Magn. Magn. Mater. **268**, 232 (2004).
[27] A. V. Kityk, M. C. Rheinstädter, K. Knorr, and H. Rieger, Phys.

Rev. B **65**, 144415 (2002).
[28] F. Alberici-Kious, J. P. Bouchaud, L. F. Cugliandolo, P. Doussineau, and A. Levelut, Phys. Rev. Lett. **81**, 4987 (1998).
[29] F. Alberici, P. Doussineau, and A. Levelut, Europhys. Lett. **39**, 329 (1997).
[30] P. Doussineau, T. Lacerda-Aroso, and A. Levelut, Europhys. Lett. **46**, 401 (1999).
[31] E. V. Colla, L. K. Chao, M. B. Weissman, and D. D. Viehland, Phys. Rev. Lett. **85**, 3033 (2000).
[32] J. Hafner and M. Krajčí, Phys. Rev. B **57**, 2849 (1998).